LEGIBILITY NOTICE

A major purpose of the Technical Information Center is to provide the broadest dissemination possible of information contained in DOE's Research and Development Reports to business, industry, the academic community, and federal, state and local governments.

Although a small portion of this report is not reproducible, it is being made available to expedite the availability of information on the research discussed herein.

LA-UR 88-2484

Los Alamos National Laboratory is operated by the University of California for the United States Department of Energy under contract W-7405-ENG-36

TITLE: COMPARISON OF LANCZOS AND SUBSPACE ITERATIONS FOR HYPERSPHERICAL REACTION PATH CALCULATIONS

LA-UR--88-2484

DE88 014402

AUTHOR(S): J. D. Kress
G. A. Parker
R. T Pack
B. J. Archer

SUBMITTED TO: Computer Physics Communications

DISCLAIMER

MASTER

Los Alamos National Laboratory
Los Alamos, New Mexico 87545

FORM NO 836 R4
ST NO 2629 5/81

Comparison of Lanczos and Subspace Iterations for Hyperspherical Reaction Path Calculations

J. D. Kress, G. A. Parker, R. T Pack and B. J. Archer***
Group T-12, MS-J569
Los Alamos National Laboratory
Los Alamos, New Mexico 87545

ABSTRACT

In an accurate treatment of 3-dimensional reactive scattering using Adiabatically-adjusting, Principal axes Hyperspherical (APH) coordinates, we obtain a 2-dimensional Schrodinger equation defined on the surface of a hypersphere. The surface Hamiltonian, which depends parametrically on the sector hyperradius ρ_h, must be diagonalized for many (100 - 200) values of ρ_h. The surface (eigen)functions are expanded in a finite element basis, where a non-uniform finite element mesh is allowed to adjust for each ρ_h. Projection of the finite element basis onto the surface Hamiltonian yields a generalized eigenvalue problem. Typically the lowest 50 - 100 eigenvalues and eigenfunctions are required at each ρ_h. Since the calculation of the surface functions is currently the expensive step for our reactive scattering procedure, it is necessary to calculate these functions as efficiently as possible. In this paper, we use both the subspace iteration and block Lanczos (with selective orthogonalization) methods to calculate the surface functions. Using both solution methods, we diagonalize the finite element matrices (of order = 1729 and of half bandwidth = 109) constructed for the $LiH + F \rightleftharpoons Li + HF$ system. CPU timings for both methods are examined as a function of the number of converged eigenvalues. Since we can generate a good initial subspace from the eigenvectors calculated at the previous value of ρ_h, we find that the subspace iteration is competitive with the Block Lanczos method when many (90) eigenvalues are calculated. We also consider a larger problem (matrices of order $\sim$ 3300 and of half bandwidth $\sim$ 135) constructed for the $F + H_2 \rightleftharpoons HF + H$ system. For this problem, we present the CPU timings required to calculate 100 eigenvalues for a sequence of five ρ_h values using the subspace iteration method.

---

* *Present Address: Department of Physics and Astronomy, University of Oklahoma, Norman, Oklahoma 73019*

** *Present Address: Department of Physics, Rice University, Houston, Texas 77251-1892*

I. INTRODUCTION

Rearrangement scattering or reactive collision processes form the heart of chemistry, and the quantum theory thereof is one of the most important unsolved problems in theoretical chemistry or theoretical molecular physics.[1] Recently, an accurate quantum theory to treat such processes has been developed using Adiabatically-adjusting, Principal axes Hyperspherical (APH) coordinates.[2] Central to this theory is the diagonalization of a 2-dimensional surface Hamiltonian which dependends parametrically on the hyperradius ρ_h. For a typical scattering system, the surface Hamiltonian must be diagonalized for many ($\sim$ 200) values of ρ_h. The surface (eigen)functions are expanded in a 2-dimensional finite element (FE) basis. The resulting surface eigenvalue problem is then solved using either the Subspace Iteration (SI) or block Lanczos method.

The outline of this paper is as follows. First, we review the APH coordinates and write down the full interaction and surface Hamiltonians. Next, we discuss the construction of the FE meshes and the functional form of each element. Examples of potential energy surfaces and selected surface functions for the $F + H_2 \rightleftharpoons HF + H$ system superimposed on non-uniform meshes are presented. Then, we provide the algorithms for the subspace iteration and block Lanczos methods. We compare CPU timings using both solution methods to solve a test problem (FE matrices of order = 1729). Finally, we present the CPU timings for a larger problem (FE matrices of order $\sim$ 3300), which reflects the size of the parameters required to provide converged surface eigenvalues, using the subspace iteration method. We then conclude with a brief discussion.

II. REACTIVE SCATTERING

In this section we briefly outline the APH reactive scattering formalism to give the reader a flavor of our approach.

A. Coordinates

Consider the generic chemical reaction for a three particle system comprised of atoms A, B and C

$$A + BC \rightleftharpoons \begin{cases} AB + C \\ AC + B \end{cases}. \tag{1}$$

We use the free particle to label the three different arrangement channels. Channel A is for the arrangement on the left-hand side of Eq. (1) and channels C and B refer to the arrangements on the right-hand side respectively. We also define i, j and k to be any cyclic permutation of the labels A, B and C.

To uniquely specify the positions of particles A, B and C for a rearrangement scattering process in a center-of-mass system requires six coordinates. A hyperspherical coordinate system consists of a hyperradius and five angular coordinates. We choose three of these hyperangles (the three Euler angles) to describe the tumbling and rotational motion of the three body system (the triangle that is defined by the positions of the three particles). For the hyperspherical coordinate system described herein we choose to align the z-axis with the smallest principle moment of inertia (this axis lies in the plane of the triatomic system). We also choose the y-axis to be perpendicular to this plane

We have specified three of the hyperspherical angles as being the Euler angles. We now define the hyperradius

$$\rho = (S_i^2 + s_i^2)^{\frac{1}{2}} \tag{2}$$

and two additional angles θ,

$$\tan\theta = \frac{[(S_i^2 - s_i^2)^2 + (2\vec{S}_i \cdot \vec{s}_i)^2]^{\frac{1}{2}}}{2S_i s_i \sin\Theta_i} \tag{3}$$

and, χ_i

$$\tan(2\chi_i) = \frac{2\vec{S}_i \cdot \vec{s}_i}{S_i^2 - s_i^2}. \tag{4}$$

These coordinates describe the relative position of the three bodies [or shape (determined by θ and χ_i) and size (determined by ρ) of the triangle]. Equations (2) and (3) are valid for any i because ρ and θ are *independent* of i. Also, for the χ_i, the three choices for i are equivalent since the χ_i differ only in a choice of origin [see Eq. (32) in Ref. (2b)]. The vectors $\vec{S}_i$ and $\vec{s}_i$ are mass scaled Jacobi vectors,[3-6] (m_i is the mass of particle i) Mass scaled Jacobi coordinates are related to the usual unscaled coordinates by

$$\vec{S}_i = d_i \left[\vec{r}'_i - \frac{m_j \vec{r}'_j + m_k \vec{r}'_k}{m_j + m_k}\right] = d_i \vec{R}_i \qquad \vec{s}_i = d_i^{-1}(\vec{r}'_k - \vec{r}'_j) = d_i^{-1}\vec{r}_i \tag{5}$$

where the scale factors, d_i, three-particle reduced mass, μ, and the total mass, M, are

$$d_i = \left[\left(\frac{m_i}{\mu}\right)\left(1 - \frac{m_i}{M}\right)\right]^{\frac{1}{2}} \qquad \mu = \left[\frac{m_A m_B m_C}{M}\right]^{\frac{1}{2}} \qquad M = m_A + m_B + m_C. \tag{6}$$

The vector $\vec{r}'_i$ in Eqs. (5) is the position of particle i in a laboratory fixed system. The vector $\vec{R}_i$ is the vector from particle i to the center-of-mass of particles j and k. Finally, $\vec{r}_i$ is the vector from particle j to particle k. [See Ref. (2b) for diagrams of the various coordinate systems].

To aid in visualizing the APH internal coordinates we note that θ represents a *bending* angle; $\theta = 0$ corresponds to oblate top triangular configurations. On the other hand, $\theta = \pi/2$ corresponds to collinear arrangements. The APH coordinates, unlike most 3D hyperspherical coordinates, reduce directly to the hyperspherical coordinates usually used in collinear model calculations. While ρ describes the overall size of the ABC system, θ and χ_i describe its shape, and it is often helpful to view things on the surface of a sphere as functions of θ and χ_i with ρ fixed. θ and χ_i cover the upper half of the surface of a sphere so that we can make plots using the projection used in maps of the earth as viewed from the north pole i.e. the *stereographic projection.*

Such a projection of a contour plot for the $F + H_2 \rightleftharpoons HF + H$ potential energy surface (PES), version 5A of ref. (7), is shown for $\rho = 7.3a_0$ in Fig. (1a). The circle on this plot is the equator of the upper half sphere. The present plot shows what happens as the system bends out of the collinear plane ($\theta < \pi/2$). At this large distance, the arrangement channels are well separated. The shaded regions are strongly repulsive regions where V > 10 eV. Motion parallel to the dotted contours represents rotation of an H_2 fragment in channel A (HF fragment in channels B and C), and motion perpendicular to these contours represents vibration of an H_2 fragment in channel A (HF fragment in channels B and C). Six channels appear in Fig.

(1) instead of 3, because behavior at $\chi \pm \pi$ is related to behavior at χ by inversion, giving each channel twice.

A similar plot at $\rho = 5.2a_0$ is shown in Fig. (1b). Motion along the equator between channels A and B, and between channels A and C, corresponds to motion across the transition state. The rotational hindering or bending potential is shown by the shape of the full contours at 1.44 eV, and of the inner contours at 2.1 and 2.8 eV, between channels A and B, and between channels A and C. These specific contours are not semicircular but consist of narrow fingers extending up the surface of the sphere from the collinear equator for 1.44 eV, and of wider fingers extending down the surface of the sphere from the pole (oblate top) for 2.1 and 2.8 eV.

B. Full interaction Hamiltonian

We must solve the time independent Schrödinger equation

$$(E - T - V)\Psi = 0 \tag{7}$$

subject to the usual scattering boundary conditions. The total energy E and interaction potential V are independent of the three Euler angles,

$$V = V(\rho, \theta, \chi_i). \tag{8}$$

The kinetic energy operator T expressed in APH coordinates, is

$$\begin{aligned} T = &-\frac{\hbar^2}{2\mu\rho^5}\frac{\partial}{\partial\rho}\rho^5\frac{\partial}{\partial\rho} - \frac{\hbar^2}{2\mu\rho^2}\left\{\frac{4}{\sin 2\theta}\frac{\partial}{\partial\theta}\sin 2\theta\frac{\partial}{\partial\theta} + \frac{1}{\sin^2\theta}\frac{\partial^2}{\partial\chi_i^2}\right\} \\ &+ \frac{J_x^2}{\mu\rho^2(1+\sin\theta)} + \frac{J_y^2}{2\mu\rho^2\sin^2\theta} + \frac{J_z^2}{\mu\rho^2(1-\sin\theta)} - \frac{i\hbar\cos\theta}{\mu\rho^2\sin^2\theta}J_y\frac{\partial}{\partial\chi_i}. \end{aligned} \tag{9}$$

Defining the first term on the right hand side of (9) to be T_ρ, and the terms in braces (including the prefactor) to be T_h, we have, $T = T_\rho + T_h + T_r + T_c$, where T_r is the rotational kinetic energy (terms with J_i^2) and T_c is the Coriolis term associated with the tumbling motion of the triatomic system. The J_i in Eq. (9) refer to the body-fixed components (z-axis aligned with the smallest principle moment of inertia) of the total angular momentum $\vec{J}$. The n^{th} solution that is regular at the origin ($\rho = 0$) is

$$\Psi^{JMn} = \sum_{t,\Lambda}\rho^{-5/2}\psi_{t\Lambda}^{Jn}(\rho)\Phi_{t\Lambda}^{J}(\theta, \chi_i; \rho_h)\hat{D}_{\Lambda M}^{J}(\alpha, \beta, \gamma) \tag{10}$$

where $\hat{D}_{\Lambda M}^{J}(\alpha, \beta, \gamma)$ are the normalized Wigner rotation matrix elements. The radial wavefunctions $\psi_{t\Lambda}^{Jn}(\rho)$ are functions of the hyperradius. The $\Phi_{t\Lambda}^{J}(\theta, \chi_i; \rho_h)$ are functions of θ and χ_i and depend parametrically on the fixed sector hyperradius. The latter functions are the surface functions, (eigenfunctions at a fixed sector hyperradius), referred to in the Introduction.

C. Surface Functions

The hyperspherical surface functions $\Phi_{t\Lambda}^{J}(\theta, \chi_i; \rho_h)$ are obtained by solving an eigenvalue equation at a fixed sector hyperradius ρ_h

$$\begin{aligned} &\left[-\frac{\hbar^2}{2\mu\rho_h^2}\left\{\frac{4}{\sin 2\theta}\frac{\partial}{\partial\theta}\sin 2\theta\frac{\partial}{\partial\theta} + \frac{1}{\sin^2\theta}\frac{\partial^2}{\partial\chi_i^2}\right\} + \frac{(A+B)}{2}\hbar^2 J(J+1)\right. \\ &\left. + \left(C - \frac{1}{2}A - \frac{1}{2}B\right)\hbar^2\Lambda^2 + V(\rho_h, \theta, \chi_i) + \frac{15\hbar^2}{8\mu\rho_h^2}\right]\Phi_{t,\Lambda}^{J} = \mathcal{E}_{t\Lambda}^{J}(\rho_h)\Phi_{t,\Lambda}^{J} \end{aligned} \tag{11}$$

or

$$H_s \Phi^J_{t\Lambda} = \mathcal{E}^J_{t\Lambda} \Phi^J_{t\Lambda} \tag{12}$$

at a large but finite collection of hyperradii $\{\rho_h\}$. In Eq. (11) A, B, and C are defined by

$$A = \frac{1}{\mu\rho_h^2(1+\sin\theta)} \qquad B = \frac{1}{2\mu\rho_h^2\sin^2\theta} \qquad C = \frac{1}{\mu\rho_h^2(1-\sin\theta)}. \tag{13}$$

The surface function Hamiltonian includes T_h and the symmetric top portion of the rotational Hamiltonian T_r. The asymmetric top portion of the rotational Hamiltonian and the Coriolis term induce coupling in the coupled-channel equations. The surface function Hamiltonian in Eq. (11) contains the full interaction potential and all diagonal angular operators. Therefore the surface functions should form a rapidly convergent basis for the coupled-channel equations, equations which must be solved in order to extract the scattering S-matrix, transition probabilities, etc. See Ref. (2b) for the details.

III. COMPUTATIONAL PROCEDURE

A. Overview

In this section we will outline the pertinent parts of our computational procedure for reactive scattering which relate to the calculation of the surface functions. First, an optimized mesh (or element definition) is constructed in program MESHER at a multitude of fixed hyperradii. This program was designed to minimize computational time, to improve the accuracy of the surface functions, and to automate the creation of input data for the surface function program. Then, the optimized mesh is employed by program SURFUNC (which is a modified version of the engineering finite element code ADINA[8]) to generate eigenfunctions and eigenvalues of the surface function Hamiltonian Eq. (11). The numerical values of these surface functions at each mesh point are essential for all of the subsequent steps. This step *currently* requires significant computer time *and* disk storage. These two steps will now be discussed in more detail.

B. Meshing

MESHER establishes an optimized mesh for the surface function program. SURFUNC requires an input mesh made up of discrete points (unique θ, χ_i pairs) called *nodes* and boundary conditions that are placed on the mesh.

For the reactions considered in this paper the potential is a function of the internal APH coordinates ρ, θ, and χ_i. The surface functions are calculated at a series of fixed ρ values on the (θ, χ_i) surface. The nodal points are specified by unique θ, χ_i coordinate pairs. We are using quadrilateral elements with 9 nodes per element. Hundreds of nonoverlapping elements of different sizes make a *mesh*.

The shape of the mesh (size of each of the elements) is determined by two conflicting characteristics of any finite element code. First, the more nodal points included in the mesh, the more accurate will be the eigenfunctions and eigenvalues. Second, the more nodal points in the mesh, the more computer time will be required to calculate the desired surface functions. The finite element code uses a polynomial in (θ, χ) space for each element as a basis for the surface functions. In regions where the amplitudes of the surface functions are large it is desirable to have as fine a mesh as one can afford. However, in the regions

where the surface functions are nearly zero one can use fairly large elements or a coarse grid. Ideally, the mesh would be very dense in the strongly attractive regions, very sparse in the very repulsive classically forbidden regions, and have a smooth transition between the two regions. To obtain this desired result we start with a very sparse mesh and then subdivide it many times, concentrating each time on the deeper part of the potential. In actual practice, we now base the subdivsion process on the root mean square (RMS) of the surface functions calculated for the previous value of ρ_h. Qualitatively, the regions of maximum RMS surface function density usually correspond to the regions of the deeper parts of the potential. But, for example, in the case of highly excited vibrational states, the surface functions can be very delocalized with respect to the wells of the potential. Therefore, basing the the mesh on the RMS of the surface functions places the nodes in *all* the regions where they are needed to accurately represent the surface functions. An optimized mesh has about 3,000 to 5,000 nodal points instead of the ≈50,000 nodal points of a uniform mesh. This procedure allows one to obtain highly accurate surface functions with minimal cost.

A mesh for the $F + H_2 \rightleftharpoons HF + H$ system superimposed on the 5A-PES and on some surface functions is shown in Fig. (2) for $\rho_h = 7.3a_0$. This mesh is one division coarser than the mesh required to give nearly converged surface eigenvalues. The 5A-PES for $F + H_2 \rightleftharpoons HF + H$ with the superimposed mesh is displayed in Fig. (2a). The dense mesh is conveniently restricted to the lower regions of the potential. Note the height of the barriers to reaction which exist between the H_2 channel (which faces the reader at $\chi_i = 0$) and the well of the HF channels (which are located at $\chi_i \sim \pm\pi/4$). The function in Fig. (2b) correlates asymptotically with the $v = 3, j = 0$ state for HF. [This function is presented on a mesh one division finer than the others in Fig. (2).] This function lacks nodes along the rotational motion path (indicative of a $j = 0$ state), and also contains an increased amount of density in the $\theta = \pi/2$ region with respect to the $\theta \cong \pi/4$ region (indicative of the preference of the three-atom system to remain collinear). The function in Fig. (2c) correlates with the a $v = 2, j = 14$ state for HF. This function has many nodes present along the rotational motion path (indicative of a high j state). Fig. (2d) correlates with the $v = 0, j = 0$ state of H_2.

Fig. (3) is similar to Fig. (2), except that now $\rho_h = 5.2a_0$, which is near the $H \cdots H \cdots F$ transition state region. In Fig. (3a), the transition state between the H_2 channel and the HF channels occurs on the collinear equator at the position of the arrows. This transition state is in the same position as the barrier described in Fig. (2a). As ρ is decreased from ∞ to $5.2a_0$ the height of the barrier decreases from a very large value to the value observed in Fig. (3a) for the transition state. The function in Fig. (3b), which corresponds to the lowest eigenvalue for this value of ρ_h, correlates with the $v = 0, j = 0$ state for HF. The effect of the strongly hindered rotational motion, discussed earlier in context with Fig. (1b), appears in Fig. (3b) along the collinear equator in the form of the increased wavefunction density for the $H \cdots FH$ collinear arrangement with respect to the $H \cdots HF$ arrangement. Figs. (3c) and (3d) are examples of some of the functions which provide reaction flux to the total wavefunction. Both functions appear to be a mix between a $v = 0$ H_2 state and a $v = 3$ HF state.

C. Surface Functions

The surface function Hamiltonian in Eq. (11) is a partial differential equation in the two variables θ and χ_i. The finite element (FE) method is used to solve this eigenvalue equation for the eigenfunctions [surface functions $\Phi^J_{i\Lambda}(\theta, \chi_i, \rho_h)$] and eigenenergies $\mathcal{E}^J_{i\Lambda}(\rho_h)$.

The FE method[9] is a powerful numerical technique for solving partial differential equations. The fundamental idea of this method is that surface functions which are continuous can be approximated by a set of piecewise-continuous polynomials defined over a finite number of subdomains called elements. A major advantage of the finite element method is that the size of the elements can be varied across the domain. Hence small elements can be used in physically accessible regions of space and large elements in physically inaccessible regions of space. Two types of elements are commonly used to model a two-dimensional domain, the triangle and quadrilateral. Originally triangular shaped elements were used almost exclusively. It is now generally accepted that the quadrilateral elements are more efficient. In each element the surface function is approximated by an interpolating polynomial. This polynomial has 9 coefficients, so the element must have 9 nodes to uniquely determine the polynomial coefficients. These nodes are at the corners of the quadrilateral, the midpoint of each of the sides, and the center of the quadrilateral. The various shapes and nodal patterns exhibited by the surface functions presented in Figs. (2) and (3) illustrate the need for a flexible basis capable of describing both localized and global topologies on the hypersphere. We believe that the FE basis described above can provide such flexibility. Although at this stage in our research we are finding that the FE basis cannot provide at a reasonable cost surface eigenvalues which are converged and consistent over the full range of ρ_h for the $F + H_2 \rightleftharpoons HF + H$ system.

The surface function eigenenergies for the lowest 20 states of $d\mu + t \rightleftharpoons t\mu + d$, the exchange of a muon between a deuteron and a triton, are plotted as a function of ρ in Fig. (4). For large values of ρ, the eigenenergies are approaching the eigenenergies of the isolated atoms $d\mu$ and $t\mu$ as one would expect.

IV. ITERATIVE METHODS

Projection of the FE basis onto Eq. (11) for a particular value of J, Λ, and ρ_h yields the generalized eigenvalue problem

$$\mathbf{H\Phi = S\Phi E} \tag{14}$$

where $\mathbf{S}$ is an overlap matrix. Since the calculation of the surface functions is currently the expensive step of our procedure, it is imperative that we solve Eq. (14) as efficiently as possible. For the matrices required for our scattering problems [order n = 3000 - 5000, half bandwidth m = 100 - 200], the method of choice is to solve Eq. (14) iteratively versus solving for the complete spectrum of $(\mathbf{H}, \mathbf{S})$.

A. Subspace Iteration

One approach used widely by the engineering community to solve problems like Eq. (14) is the Subspace Iteration (SI) method. The version of SI implemented in our scattering code was obtained from the ADINA engineering package.[9] The iteration is started by choosing a set of q vectors, represented as the columns of $\mathbf{X_1}$, which span the starting subspace. Constructing $\mathbf{X_1}$ from a good estimate to the eigenvectors of Eq. (14) greatly enhances the convergence rate, as we shall show later. Usually the subspace size is chosen according to standard practice[9] as $q = max(2p, p+8)$ where p = number of desired eigenpairs.

Before iterating, $\mathbf{H}$ is factored as $\mathbf{LDL^T}$ to facilitate the linear equation solution step. Then the algorithm proceeds[9] for $k = 1,2,\ldots$ (the subscripts denote the k^{th} iteration):

1. Solve: $\mathbf{HY_{k+1}} = \mathbf{SX_k}$.
2. Form the projected matrices:
   $\mathbf{H'_{k+1}} = \mathbf{Y^T_{k+1}HY_{k+1}}$ and $\mathbf{S'_{k+1}} = \mathbf{Y^T_{k+1}SY_{k+1}}$.
3. Solve the projected $(p \times p)$ eigenvalue problem using the generalized Jacobi method:
   $\mathbf{H'_{k+1}\Phi'_{k+1}} = \mathbf{S'_{k+1}\Phi'_{k+1}E'_{k+1}}$.
4. Update the approximation: $\mathbf{X_{k+1}} = \mathbf{Y'_{k+1}\Phi'_{k+1}}$.
5. Check $\mathbf{E'_{k+1}}$ for convergence of the lowest p eigenvalues. Iterate back to step 1 if necessary.

The procedure converges; that is $\mathbf{E'_{k+1}} \rightarrow \mathbf{E}$ and $\mathbf{X_{k+1}} \rightarrow \mathbf{\Phi}$ as $k \rightarrow \infty$.

B. Block Lanczos

The second iterative method we considered for solving Eq. (14) is the block Lanczos reduction algorithm.[10] Although a Lanczos algorithm could be designed to solve the *generalized* eigenvalue problem directly, the Lanczos package[11] we used is based upon the block Lanczos reduction for an *ordinary* eigenvalue problem. We therefore convert Eq. (14) to an ordinary eigenvalue problem using a spectral transformation of the form as suggested by Ericsson and Ruhe.[12] The transformed problem is then solved using the Lanczos method, with the solutions to Eq. (14) obtained by a back-transformation. The idea behind the transformation is to invert the spectrum of Eq. (14). This inversion spaces the transformed spectrum "hyperbolically" [see Ref. (12)] which allows for a more efficient calculation since the eigenvalues will be more distinct. Specifically we form the transformed matrix

$$\mathbf{H'} = \mathbf{D^{-1/2}L^{-1}SL^{-T}D^{-1/2}} \tag{15}$$

where $\mathbf{H}$ is factored as $\mathbf{LDL^T}$. We then solve the transformed problem

$$\mathbf{H'\Phi'} = \mathbf{\Phi'E'} \tag{16}$$

using Lanczos. The spectrum and eigenvectors of Eq. (16) are related to those of Eq. (14) by

$$E'_i = 1/E_i \qquad \textit{and} \qquad \mathbf{\Phi'} = \mathbf{D^{1/2}L^T\Phi}. \tag{17}$$

Since the Lanczos algorithm only requires the formation of a matrix $\mathbf{U} = \mathbf{H'V}$ upon input of $\mathbf{V}$, Eq. (15) is never constructed explicitly. Instead $\mathbf{U}$ is formed from $\mathbf{L}$,$\mathbf{D}$, and $\mathbf{S}$ using linear equation solves and a matrix multiplication.

The central result of the block Lanczos procedure is to reduce $\mathbf{H'}$ to a block tridiagonal form $\mathbf{T_k} = \mathbf{Q_k^T H' Q_k}$. $\mathbf{Q_k}$ is constructed as $(\hat{\mathbf{Q}}_1, \hat{\mathbf{Q}}_2, \ldots \hat{\mathbf{Q}}_k)$ where each $\hat{\mathbf{Q}}_k$ is a block of n_b column vectors (n_b is defined as the Lanczos block size). $\mathbf{Q_k}$ forms a distinguished basis for the Krylov subspace $\mathcal{K}^k(\hat{\mathbf{Q}}_1) = \mathbf{span}[\mathbf{Q}_1, \mathbf{H'}\hat{\mathbf{Q}}_1, (\mathbf{H'})^2\hat{\mathbf{Q}}_1, \ldots (\mathbf{H'})^{k-1}\hat{\mathbf{Q}}_1]$. Explicitly,

$$\mathbf{T_k} = \begin{pmatrix} \mathbf{A_1} & \mathbf{B_1^T} & \mathbf{0} & \mathbf{0} \\ \mathbf{B_1} & \mathbf{A_2} & \ddots & \mathbf{0} \\ \mathbf{0} & \ddots & \ddots & \mathbf{B_{k-1}^T} \\ \mathbf{0} & \mathbf{0} & \mathbf{B_{k-1}} & \mathbf{A_k} \end{pmatrix} \tag{5}$$

where the $\mathbf{A_k}$ and $\mathbf{B_k}$ are of order n_b. If $n_b = 1$, one recovers the simple Lanczos reduction scheme where: 1) $\mathbf{Q_k} \rightarrow \mathbf{q_k}$, a single column vector; 2) $\mathbf{A_k} \rightarrow \alpha_k$ and $\mathbf{B_k} \rightarrow \beta_k$, both constants, and; 3) $\mathbf{T_k}$ becomes strictly tridiagonal. The $\hat{\mathbf{Q}}_\mathbf{k}$ are constructed iteratively once a starting residual $(n \times n_b)$ matrix $\mathbf{R_0}$ ($\|\mathbf{R_0}\| \neq \mathbf{0}$) is specified. Then the algorithm[10] proceeds for $k = 1, 2, \ldots$ (again, the subscripts denote the k^{th} iteration):

1. Orthonormalize $\mathbf{R_{k-1}}$ (QR factorization): $\mathbf{R_{k-1}} = \hat{\mathbf{Q}}_\mathbf{k}\mathbf{B_{k-1}}$
2. $\mathbf{R_k} \leftarrow \mathbf{H}'\hat{\mathbf{Q}}_\mathbf{k} - \hat{\mathbf{Q}}_\mathbf{k-1}\mathbf{B}_\mathbf{k-1}^\mathbf{T}$ $(\hat{\mathbf{Q}}_\mathbf{0} = \mathbf{0})$.
3. $\mathbf{A_k} \leftarrow \hat{\mathbf{Q}}_\mathbf{k}^\mathbf{T}\mathbf{R_k}$.
4. $\mathbf{R_k} \leftarrow \mathbf{R_k} - \hat{\mathbf{Q}}_\mathbf{k}\mathbf{A_k}$.
5. Solve using Rayleigh Quotient Iteration: $\mathbf{T_k\Theta_k} = \mathbf{\Theta_k E_k}$.
6. Check $\mathbf{E_k}$ for convergance of the p lowest eigenvalues. Iterate back to step 1 if necessary.

The eigenvectors of $\mathbf{H}$ are obtained via Eq. (17) as $\mathbf{\Psi} = \mathbf{L}^{-\mathbf{T}}\mathbf{D}^{-1/2}\mathbf{Q_k\Theta_k}$.

The advantage to using the block Lanczos (as well as the disadvantage to using simple Lanczos) is the property that the Lanczos reduction can only determine degenerate roots of multiplicity n_b. Certainty in determining degenerate eigenvalues requires a value of n_b one greater than the expected maximum degeneracy in the problem. This choice prevents errors from accidental degenercies due to numerical tolerances, crossings of adiabatic eigenvalues, etc. The version of Lanczos implemented in our scattering code was derived from the SNLASO code of Scott.[11] This code finds the eigenvalues at either end of the spectrum using the block Lanczos reduction in conjunction with the selective orthogonalization (SO) technique. The Lanczos reduction breaks down if $\|\mathbf{I} - \mathbf{Q}_\mathbf{k}^\mathbf{T}\mathbf{Q_k}\|$ deviates from zero ($> \epsilon$) due to numerical roundoff. Using Paige's theorem,[13,10] it has been shown[14] that purging the residual $\mathbf{R_k}$ in step 4 of the converged eigenvectors determined from the previous iteration at step 5 maintains the linear independence of the columns of the $\mathbf{Q_k}$. The SO can be inserted as step 4.5 in the algorithm. [See Refs. (10) and (14) for more details].

V. TEST PROBLEM: *LiH + F*

One three body reactive scattering system of interest is $LiH + F \rightleftharpoons Li + HF$. A bond order PES for this system has been constructed by Laganà and coworkers[15a] fit to the *ab initio* energies of Chen and Schaefer.[15b] Using this PES, the FE solution to Eq. (11) for $J = \Lambda = 0$ has been calculated at two values of ρ_h, ($\rho_1 = 5.0a_0$ and $\rho_2 = 5.1a_0$). A uniform FE mesh was constructed. This mesh was chosen for test purposes only, and is in no way an optimal choice for a mesh. (See Sec. III. B.) The $\mathbf{H}$ and $\mathbf{S}$ obtained are of order $n = 1729$ and half bandwidth $m = 109$. (The half bandwidths quoted in this paper are average values, since the symmetric matrices are stored in a skyline format.[9] The average half bandwidth of a symmetric matrix is defined here as the number of matrix elements between the diagonal and the skyline, inclusive, divided by the order n.)

The resulting generalized eigenvalue problem was then solved using both the SI and the block Lanczos (BL) methods for both values of ρ_h. Within the SI method, two variations with regards to the choice of the starting subspace $\mathbf{X_1}$ were attempted. In one case, $\mathbf{X_1}$ at both values of ρ_h was construced from

random vectors [which we denote as SI(random)]. In the other case, $\mathbf{X_1}$ was constructed from random vectors for ρ_1, but then $\mathbf{X_1}$ for ρ_2 was constructed from the eigenvectors obtained at ρ_1 [which we denote as SI(good)]. If we consider the difference in Eq. (14) evaluated at ρ_1 and at ρ_2 as a perturbation, we may expect the eigenvectors from ρ_1 to be a "good" approximation to the span of the subspace for the eigenvectors at ρ_2. This has been verified by comparing the eigenvalues at both ρ_h values, and we find this perturbation argument to be valid. In practice, the eigenvectors from the previous ρ_h are available to us at no cost, since the solution to our scattering problem requires us to calculate the eigenfunctions to Eq. (1) sequentially in ρ_h for a set of 100 - 200 values of ρ_h.

B. Few eigenvalue regime

In Fig. (5) we present the amount of CPU time required to diagonalize the $LiHF$ problem plotted as a function of p for $p < 20$ (the "few eigenvalue" regime). (The CPU times quoted through out this paper were determined on a CRAY-XMP.) Three approaches are presented: BL with $n_b = 2$; SI(random); and SI(good). For $p = 20$, BL outperforms both SI(random) and SI(good) by a factor of ~ 4 and of ~ 3, respectively. Note also that although both the SI and BL results appear to scale linearly in p, the BL curve is of lesser positive slope than either SI curve. If this linearity held for large p, (it does not as we shall see later) the BL method would still appear to be more efficient than SI(good) by a factor of ~ 3 - 4.

A similar scaling with respect to p was also observed in the few eigenvalue regime by Nour-Omid, Parlett, and Taylor[16] (hereafter referred to as NPT). NPT considered the FE solution for a structure which when parameterized yielded matrices corresponding to $\mathbf{H}$ and $\mathbf{S}$ of order $n = 468$ and of $m = 45$. In Fig. (6) of Ref. (16), NPT plot as a function of p ($p \leq 9$) the number of matrix-vector operations (MVOPs) required to diagonalize their problem using both SI(random) and BL with $n_b = 1$ and 2. NPT defined a MVOP as a $\mathbf{LDL^T}$ solve plus a matrix multiply for a *single* column vector. Using this measure, step 1 of the SI algorithm costs q MVOPs per iteration, whereas step 2 of the BL algorithm costs only n_b MVOPs per iteration. In Fig. (6) of NPT, the total MVOPs scaled ~linearly for both BL and SI, with the SI curve increasing much more steeply than the BL curve. This case parallels the behavior observed in our Fig. (5) for BL *vs.* SI(random). Thus, NPT correctly concluded that the BL method was by far more efficient than using SI for solving problems in the few eigenvalue regime, as long as a good initial subspace is *not* available.

B. Many eigenvalue regime

Implicit in the above analysis is the assumption that the MVOPs are the rate limiting step in both algorithms. The step in each algorithm which competes with the MVOPs is: 1) the solution of the projected generalized eigenvalue problem required at each iteration of the SI method (step 3); and, 2) the solution of the reduced ordinary eigenvalue problem required at each iteration of the BL method (step 5). At the k^{th} iteration of the SI algorithm, the eigenvalue problem is of order q, *independent* of the value of k. At the k^{th} iteration of the BL algorithm, the eigenvalue problem is of order $(k \cdot n_b)$; the size of the problem increases as a function of k. Eventually for a large value of p (which requires a large number of k iterations), the cost to diagonalize the reduced eigenvalue problem exceeds the cost of the $\mathbf{LDL^T}$ solve in the BL algorithm.

This crossover of the rate determining step in the BL algorithm is apparent in Fig. (6a) where we have plotted the CPU times vs. p in the "many eigenvalue" regime (p = 20-90). The SI(good) and BL curves are approximately parallel to each other and are increasing as $\sim$ quadratic as a function of p (which we verified using a least squares fit of the data). The linear scaling observed in Fig. (5) for the few eigenvalue regime does *not* hold in the many eigenvalue regime for either method. For BL, the total cost in multiplicative operations (OPs) for the Rayleigh Quotient Iteration (step 5) scales as cubic in the leading term of p. This cost eventually approaches and overtakes the cost of the MVOPs which scales linearly in p for the number of OPs. (The OP counts assume that the total number of iterations (k_{max}) required to converge p eigenvalues scales as linear in p. Through experience we have found that $k_{max} \sim 3 \cdot p$.)

The values reported in Fig. (6a) for BL were obtained using a modified version of the original SNLASO code, where step 5 of the algorithm was made more efficient. In the few eigenvalue regime only a negligible decrease in CPU time was observed for p = 20 with respect to the original SNLASO code. Whereas in the many eigenvalue regime, a $\sim$ 30% decrease in CPU time was obtained for p = 90. Further research has provided a BL code which is $\sim$ 2.2 times faster than the original SNLASO code for p = 100 (see the accompanying paper[17] in this issue). But these further modifications have rendered the algortihm more sensitive to the loss of orthogonality in the $\mathbf{Q_k}$ such that the further modified version is not reliable enough to use when generating sets of eigenfunctions for our scattering calculations. We also note that the SI routine was used in an accelerated mode.[18] One consequence of the acceleration is to deflate converged eigenvectors from the the subspace $\mathbf{X_k}$ as they are found. This reduces the size of the subspace at nearly every iteration, which in turn decreases the order of the projected eigenproblem which is solved. As k increases, the amount of work needed to solve the projected eigenvalue problem *decreases*, which is exactly *opposite* of the behavior of the BL algorithm.

1. Good starting subspaces

Also evident in Fig. (6a) is the effect of providing a "good" starting subspace for the SI method. At p = 90, the savings in time is over a factor of 2 with respect the use of a random starting subspace [SI(good) vs. SI(random)]. In principle, a good guess to the starting Lanczos residual matrix $\mathbf{R_0}$ should also increase the convergence of the BL method. We have tested two different ways to introduce the eigenvectors from the previous ρ_h value into the $\mathbf{R_0}$ for the present ρ_{h+1} value. First, we tried constructing the n_b columns of $\mathbf{R_0}$ as linear combinations of all of the p converged eigenvectors calculated at ρ_h. This approach showed a negligible increase in convergence speed with respect to using a random block of vectors for $\mathbf{R_0}$. Second, we placed the eigenvectors associated with the n_b lowest eigenvalues calculated at ρ_h one-by-one in each column of $\mathbf{R_0}$. For a given value of p, this provided on the average about a 5% increase in the convergence speed with respect to the use of random vectors (even for p = 90). The latter procedure showed some improvement because it allowed for the projection of the n_b lowest eigenvalues at the first step of the Krylov subspace generation, i.e. $\hat{\mathbf{Q}}_2 \propto \mathbf{H}'\mathbf{R_0} \approx \mathbf{R_0}\mathbf{E}'$. Thus the n_b lowest eigenvalues converge quickly, but $(p - n_b)$ eigenvalues must still be found on subsequent iterations.

2. Variation of block size

The BL results reported in Fig. (6a) were *not* calculated with the same value of n_b for each value of p. Fig. (6b) shows the value of n_b used as a function of p. For values of $p > 50$, we found that fixing $n_b = 2$ resulted in a loss of orthogonality of the $\mathbf{Q_k}$ matrix, even within the application of the SO procedure. We can explain this behavior by assuming that a $\mathbf{Q_{k'}}$ matrix of a minimum order $k' = (k \cdot n_b)$ is needed to adequately converge p eigenvalues. If k' is large and n_b is small, a large number of k iterations must be performed. Each iteration introduces round-off error which eventually accumulates to an amount too large for the SO to correct. To decrease the number of iterations for a fixed value of k' (thus decreasing the accumulated round-off error), we must increase n_b.

Taking the above argument to an extreme, we might assume that n_b should be set as large as possible so to decrease the number of total itertations. In practice this is *not* true. We have verified that using the smallest value of n_b such that non-orthogonality is avoided yields the fastest solution for a given value of p. Even though k decreases, the order of the reduced eigenvalue problem $= (k \cdot n_b)$ increases by n_b each iteration. Thus, the work to diagonalize the increasingly larger eigenvalue problem offsets the decreased number of iterations. Each value of n_b in Fig. (6b) is the minimum value (in increments of 2) which does not introduce non-orthogonality for a given value of p.

C. Summary

In summary, for the few eigenvalue regime ($p < 20$) the dominant operational cost for both solution methods resides in the MVOP step. With SI requiring $q = max(2p, p + 8)$ MVOPs and BL requiring n_b MVOPs per iteration, respectively, the BL method is more efficient. For the many eigenvalue regime ($20 < p < 90$), the cost of solving the reduced eigenvector problem becomes competitve with the cost of the MVOPs in the BL algorithm. Therefore, the overall costs in BL are only a factor of ~ 2 less than the costs to use SI for many eigenvalue regime.

VI. PRODUCTION EXAMPLE: $F + H_2$

When we generate scattering information (a production run), we must calculate the surface functions sequentially in ρ_h for many values of ρ_h. The sequence must not be broken as we accumulate the overlap between functions functions evaluated at ρ_h and at ρ_{h+1} and not the functions themselves. We have found that the SI method is much more reliable than the block Lanczos method with respect to determining this sequence of surface functions. The block Lanczos method is sensitive to the choice of n_b and tends to fail due to a loss of orthogonality. A failure occuring at some point during a production run is not acceptable.

With the last paragraph in mind, we present the CPU times for the first five values of ρ_h from a production run in Table I using the SI method. Using the 5A-PES for the $F + H_2 \rightleftharpoons HF + H$ system, we constructed the FE matrices for $J = \Lambda = 0$ using a non-uniform mesh of the type discussed in Sec. III. B. We required $p = 100$ converged and carried an extra 50 unconverged eigenfunctions for each value of ρ_h, resulting in a subspace of size $q = 150$. This choice for q was larger than the value dictated by standard practice, but the extra functions were needed to complete the basis for the scattering calculations. In Table I we present the CPU times required to solve Eq. (14) for sucessive values of ρ_h using the SI method. Except for ρ_1, the starting subspace $\mathbf{X_1}$ was constructed from the eigenvectors calculated at the

previous ρ_h. A random guess for $\mathbf{X_1}$ was used at ρ_1. The benefits of having a "good" starting subspace is evident in Table I. Nearly a 50% savings in time is realized between the calulations at ρ_1 and ρ_3, an amount magnified by the fact that the matrices at ρ_1 are $\sim$ 50% smaller than those at ρ_3 (n = 2081 vs. n = 3301). (The difference in n is due to the fact that a coarse uniform mesh is used for ρ_1, whereas a finer and more localized mesh is used for subsequent ρ_h values. The choice of non-uniform mesh is based on the eigenfunctions of the previous ρ_h, therefore a "guess" mesh is needed for ρ_h.) One reason for the tremendous time savings is the decrease in total number of iterations k_{max} (16 vs. 52 for ρ_1 vs. ρ_2). Table I also shows the stability of the SI(good) method with respect to a change in ρ_h. The CPU times for the last three ρ_h values are within 5% of each other. The time at ρ_2 is larger than the last three values because the starting subspace generated from the eigenvectors at ρ_1 on the coarse mesh is not as good as the starting subspace obtained from the eigenvectors calculated on the finer non-uniform meshes.

VII. CONCLUSIONS

We considered the finite element solution to the surface eigenvalue problem derived from an accurate treatment of 3-dimensional scattering formulated using APH coordinates. Examples of potentials, surface functions, and non-uniform meshes plotted on the surface of the hypersphere were displayed. Both the subspace iteration (SI) and block Lanczos (with selective orthogonaliztion, BL) method were utilized to calculate surface functions. Although the SI method is slower than the BL method in the many ($\sim$ 90) eigenvalue regime, we use the SI method exclusively when determing the surface functions for a scattering production run. The SI method is less sensitive than the BL method with respect to the choice of initial parameters for each method.

We are presently considering other approaches for solving the surface eigenvalue problem which are fundamentally different than the finite element method. For some scattering systems (i.e., $F + H_2 = HF + H$), we have found that a very fine mesh is required to converge the surface eigenvalues, especially for highly excited vibrational and/or rotational surface functions. A fine mesh translates into finite element matrices which are too large (too expensive) to diagonalize even with the iterative procedures considered here in this paper. We are presently investigating the expansion of the surface functions in both an analytic basis and a discrete variable representation[19] basis. The matrices associated with these approaches should be sufficientiy small[20] that the full surface eigenvalue spectrum for many values of ρ_h can be obtained at a reasonable cost.

ACKNOWLEDGMENTS

We thank William A. Cook for much assistance with the finite element program and Susan B. Woodruff for much assistance with the implementation and optimization of the Lanczos code. This work was performed under the auspices of the U. S. Department of Energy and was partially supported by the National Science Foundation under Grant No. CHE-8706385.

REFERENCES

[1] See Chemical and Engineering News, Oct. 14 1985, pp. 9f.

[2] a) R. T Pack, *Chem. Phys. Lett.* **108**, 333 (1984); b) R. T Pack and G. A. Parker, *J. Chem. Phys.* **87**, 3888 (1987).
[3] L. M. Delves, *Nucl. Phys.* **9**, 391 (1959); **20**, 275 (1960).
[4] F. T. Smith, *J. Chem. Phys.* **31**, 1352 (1959); *Phys. Rev.* **120**, 1058 (1960).
[5] J. O. Hirschfelder and J. S. Dahler, *Proc. Nat. Acad. Sci.* **42**, 363 (1956); D. W. Jepsen and J. O. Hirschfelder, *ibid.* **45**, 249 (1959).
[6] J. O. Hirschfelder, *Intern. J. Quantum Chem. Symp.* **3**, 17 (1969).
[7] R. Steckler, D. G. Truhlar, and B. C. Garrett, *J. Chem. Phys.* **82**, 5499 (1985); F. B. Brown, R. Steckler, D. W. Schwenke, D. G. Truhlar, and B. C. Garrett, *ibid.*, 188 (1985).
[8] K. J. Bathe, *Massuchusettes Institute of Technology, Acoustics and Vibration Laboratory report 82448-1 (revision of December 1978).*
[9] K. Bathe and E. L. Wilson, *Numerical Methods in Finite Element Analysis* (Prentice-Hall, New York, 1976).
[10] B. N. Parlett, *The Symmetric Eigenvalue Problem* (Prentice-Hall, Englewood Cliffs, NJ, 1980).
[11] T. Ericsson and A. Ruhe, *Math. Comp.* **35**, 1251 (1980).
[12] D. S. Scott, *Oak Ridge National Laboratory, report CSD-48, (1979).* This reference contains the documentation for the basic SNLASO code. The code we used, which was obtained from the *netlib* library at Argonne National Laboratory, is a modified version of the Oak Ridge code modified by D. S. Scott while he was at the University of Texas.
[13] C. C. Paige, Thesis, Univ. of London, 1971; *J. Inst. Math. Appl.* **18**, 341 (1976).
[14] B. N. Parlett and D. S. Scott, *Math. Comp.* **33**, 217 (1979).
[15] a) A. Laganà, E. Garcia, and O. Gervasi, *Faraday Discuss. Chem. Soc.* **84** (1987); b) M. M. L. Chen and H. F. Schaefer, *J. Chem. Phys.* **72**, 4376 (1980).
[16] B. Nour-Omid, B. N. Parlett, and R. L Taylor, *Int. J. Num. Meth. Eng.* **19**, 859 (1983).
[17] J. D. Kress, S. B. Woodruff, G. A. Parker, and R. T Pack, *Comp. Phys. Comm.*, this issue.
[18] K. J. Bathe and S. Ramaswamy, *J. Comp. Meth. Appl. Mech. Eng.* **23**, 313 (1980).
[19] J. V. Lill, G.A. Parker, and J. C. Light, *Chem. Phys. Lett.* **89**, 483 (1982); J. C. Light, I. P. Hamilton, and J. V. Lill, *J. Chem. Phys.* **82**, 1400 (1985).
[20] Z. Bačić, private communication.

Table I. Subspace Iteration method.
$p = 100$ converged eigenvalues.
$q = 150$ vectors in subspace.

h	ρ_h (a_0)	n^a	m^a	k^b_{max}	CPU time[c] (sec)
1	4.000	2081	98	52	783
2	4.020	3277	134	20	457
3	4.040	3301	135	16	367
4	4.064	3325	136	16	359
5	4.093	3407	137	16	394

[a]Order (n) and half bandwidth (m) of **H** and **S**.
[b]Total number of iterations.
[c]CPU time on a CRAY-XMP.

FIGURE CAPTIONS

Figure 1. **a)** Stereographic projection of a contour plot of the $F + H_2 \rightleftharpoons HF + H$ 5A-PES[30] as a function of θ and χ_i on the surface of the sphere with $\rho = 7.3a_0$. All contours are measured from the bottom of the asymptotic well for HF; dashed contours are at 0.35, 0.75, 1.44 (a little above the bottom of the asymptotic well for H_2), 2.1, and 2.8 eV. The shaded regions lie above 10.0 eV. The distance from the center of the plot (north pole) is a measure of θ, and the azimuthal angle χ_i is measured from the positive x axis. Arrangement channel A is near $\chi_i = 0$, B is near $-3\pi/4$, and C is near $3\pi/4$. The channels at $\pi, \pi/4$ and $-\pi/4$ are A, B, and C, respectively plus inversion. **b)** Same as Fig. a) except with ρ fixed at 5.2 a_0. The transition states are the small barriers along the equator (on the circle) located near $\pi/6$, $-\pi/6$, $5\pi/6$, and $-5\pi/6$.

Figure 2. **a)** Perspective plots of the 5A-PES[7] for the $F + H_2 \rightleftharpoons HF + H$ system at a hyperradius of $7.3a_0$. A H_2 channel, centered at $\chi_i = 0$, faces the reader. Two of the HF channels are centered near $\chi_i = \pm\pi/4$. θ runs from zero (the central point of the mesh) to $\pi/2$ (the circular boundary of the mesh). The potential is clipped at 5 eV (at the plateaus) and the zero of energy is relative to the HF asymptotic well. The arrows point at the barriers between the H_2 channel and the HF channels. **b)** The surface function $\Phi^0_{56,0}(\theta, \chi_i; \rho_h)$ at $\rho_h = 7.3a_0$. A finer mesh with respect to the others is used here. The coordinate system is the same as that in Fig. a). **c)** The surface function $\Phi^0_{59,0}(\theta, \chi_i; \rho_h)$ at $\rho_h = 7.3a_0$. The coordinate system is the same as that in Fig. a) **d)** The surface function $\Phi^0_{60,0}(\theta, \chi_i; \rho_h)$ at $\rho_h = 7.3a_0$. The coordinate system is the same as that in Fig. a).

Figure 3. **a)** Perspective plots of the 5A-PES[7] for the $F + H_2 \rightleftharpoons HF + H$ system at a hyperradius of $5.2a_0$. The coordinate system and energy scale is the same as that used in Fig. (2). The arrows point at the transition state regions between the H_2 channel and the HF channels. **b)** The surface function $\Phi^0_{1,0}(\theta, \chi_i; \rho_h)$ at $\rho_h = 5.2a_0$. The coordinate system is the same as that in Fig. a). **c)** The surface function $\Phi^0_{63,0}(\theta, \chi_i; \rho_h)$ at $\rho_h = 5.2a_0$. The coordinate system is the same as that in Fig. a). **d)** The surface function $\Phi^0_{64,0}(\theta, \chi_i; \rho_h)$ at $\rho_h = 5.2a_0$. The coordinate systemis the same as that in Fig. a).

Figure 4. Plot of the surface function eigenvalues in eV for $d\mu + t \rightleftharpoons t\mu + d$ as a function of hyperradius ρ in a_0.

Figure 5. CPU time required to converge p eigenvalues for the $LiH + F \rightleftharpoons Li + HF$ test problem. ○ = SI(random), △ = SI(good), + = BL with $n_b = 2$.

Figure 6. **a)** CPU time required to converge p eigenvalues for the $LiH + F \rightleftharpoons Li + HF$ test problem. ○ = SI(random), △ = SI(good), + = BL. The values of SI(random) for $p = 80$ and 90, which are off scale, are 358 and 551 sec, respectively. **b)** Block size used to generate the BL results in Fig. a).

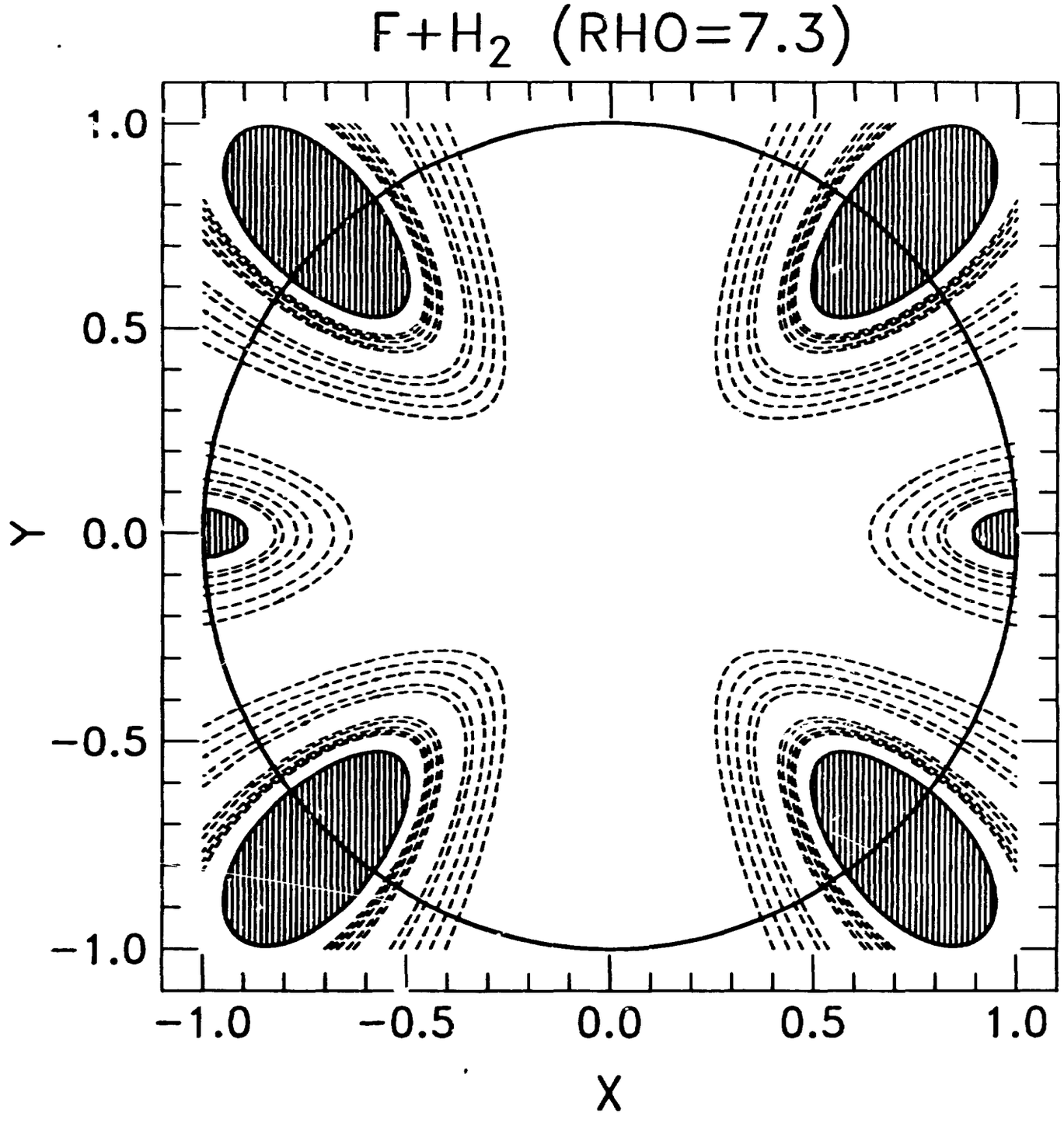

Fig. 2a

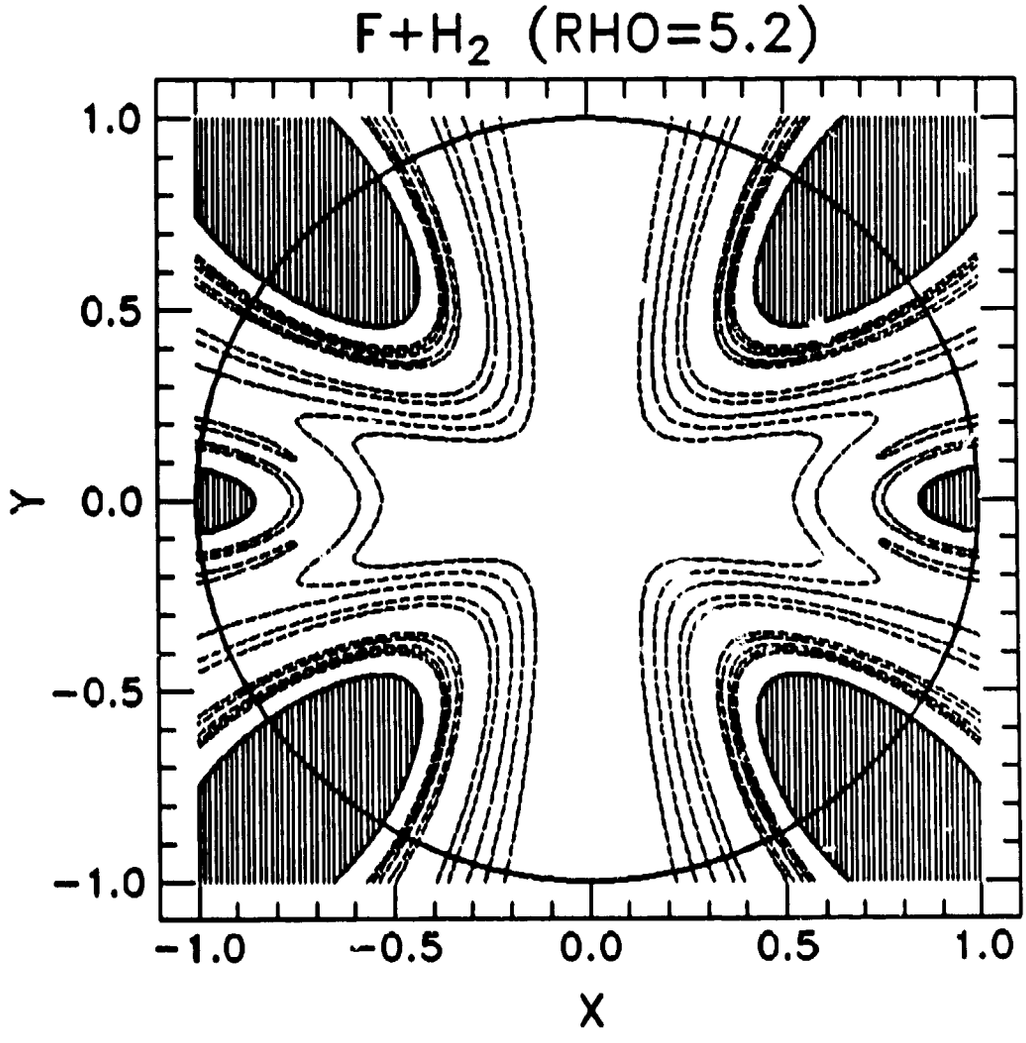

Fig 16

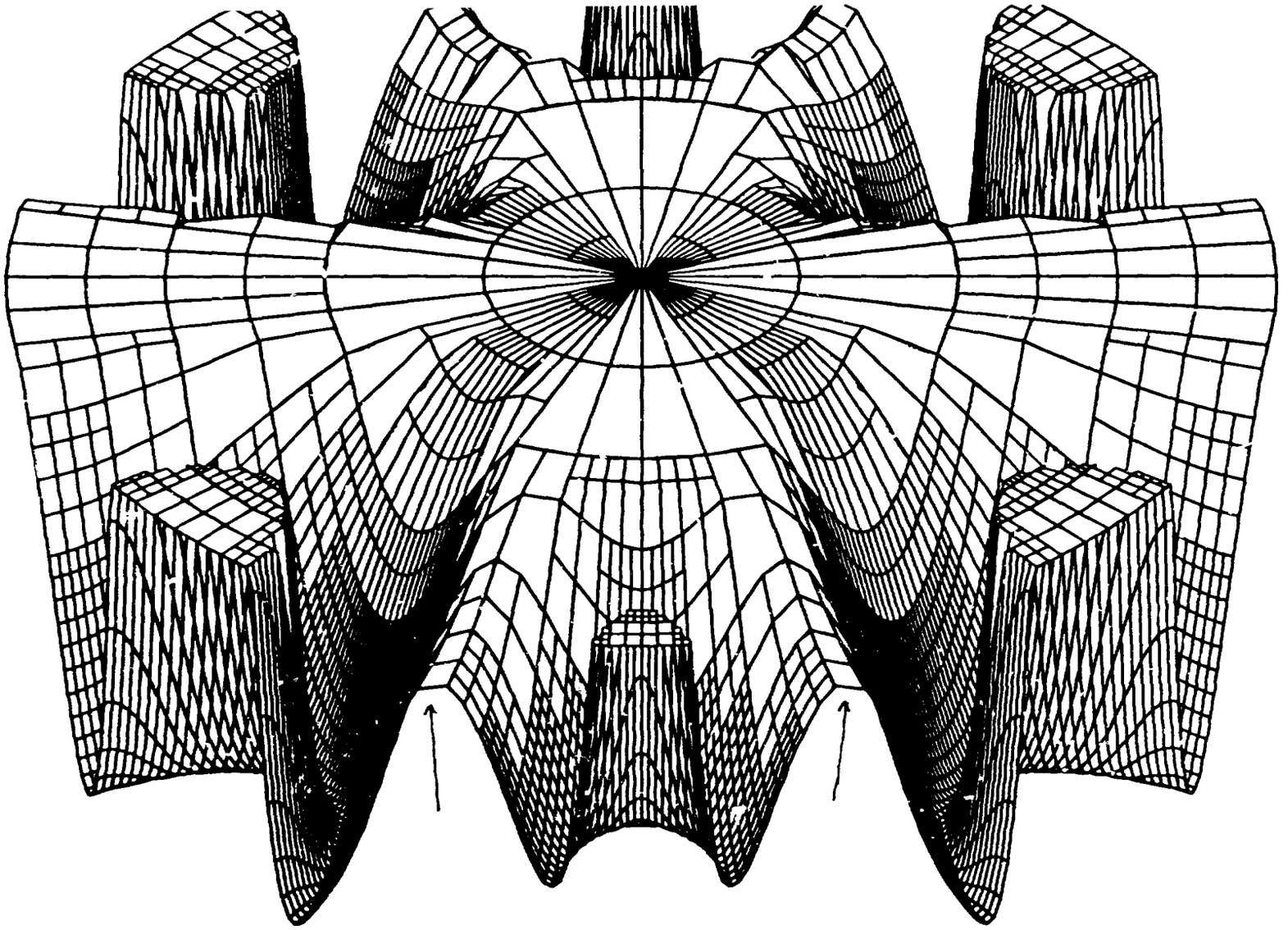

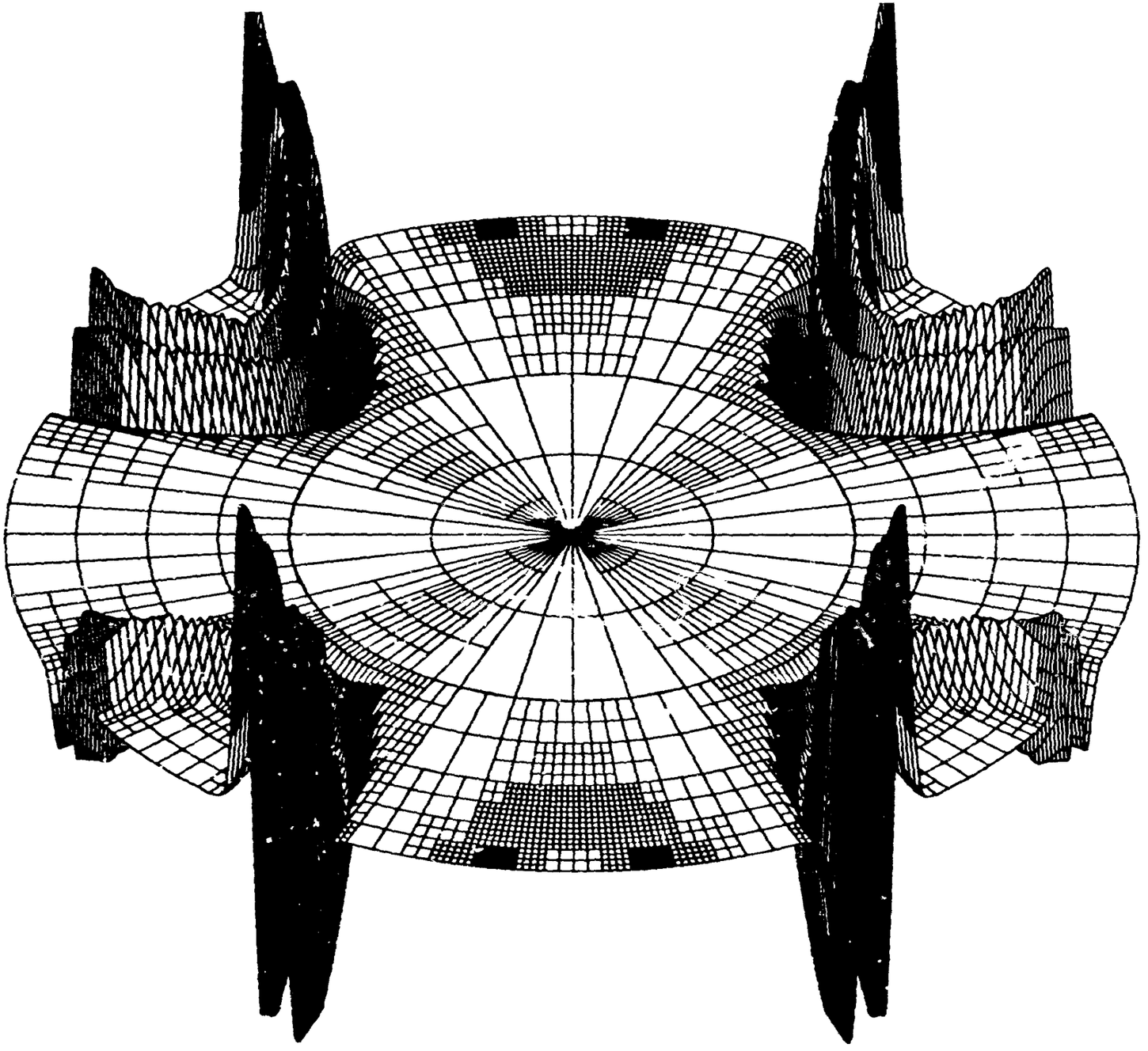

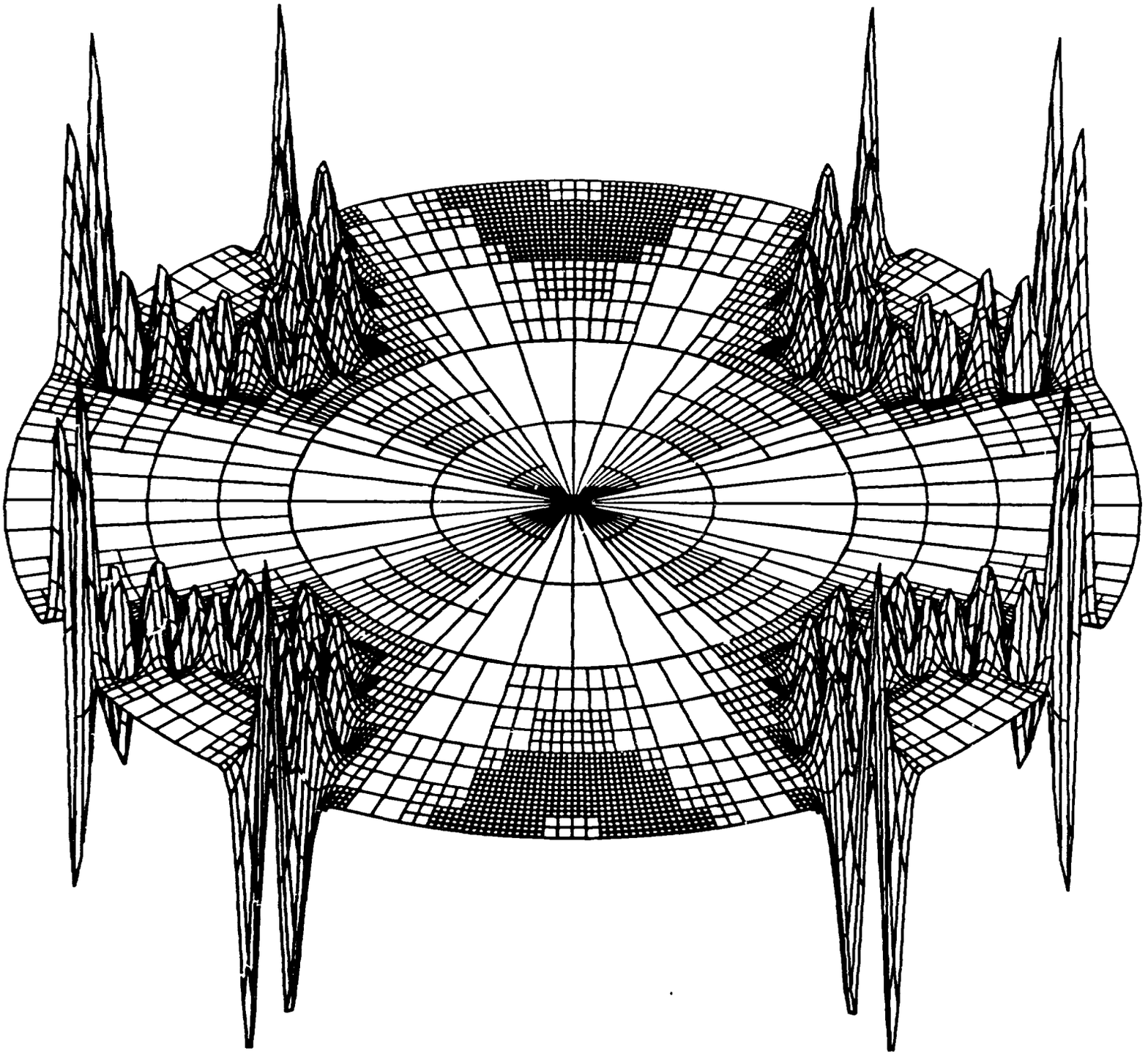

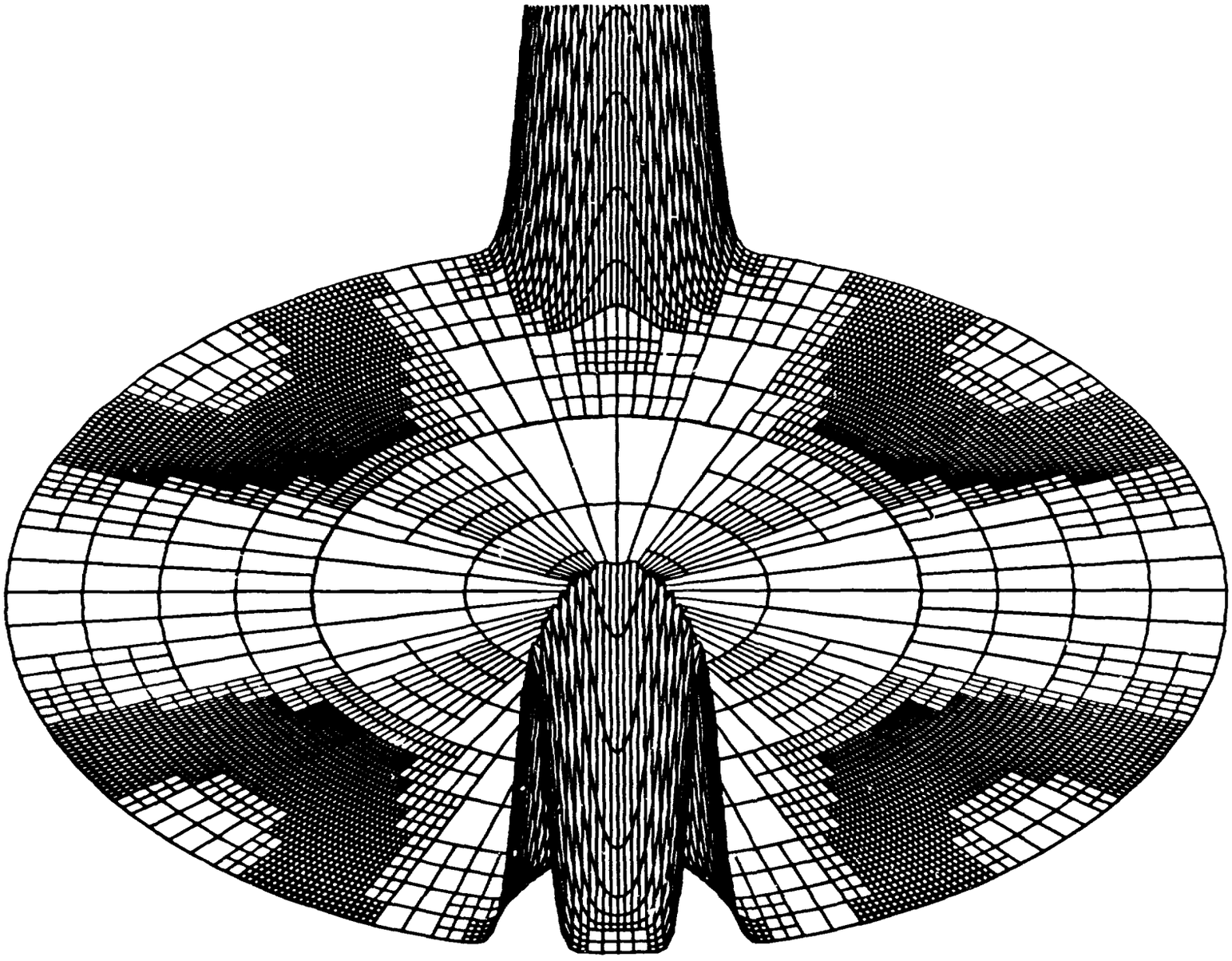

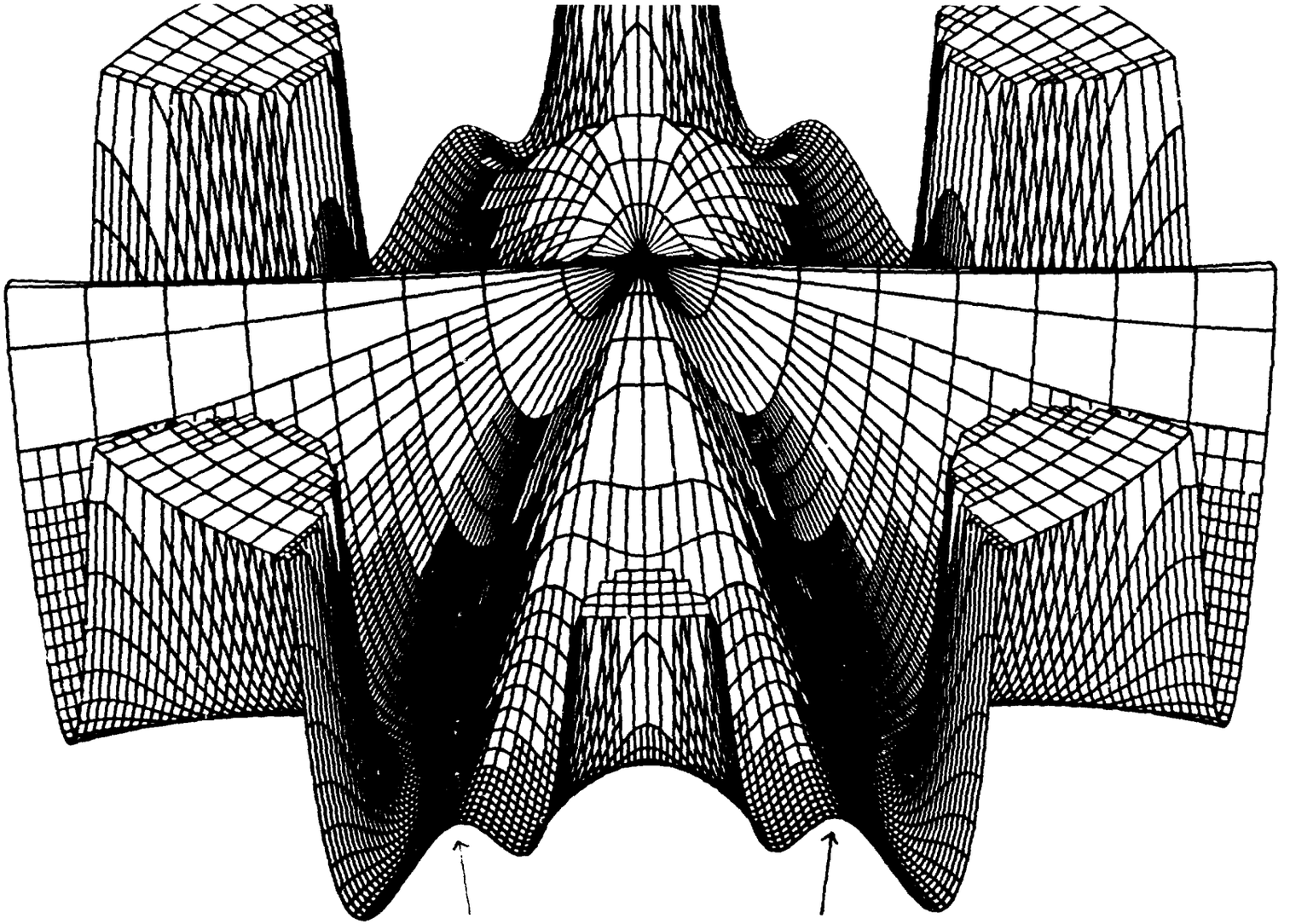

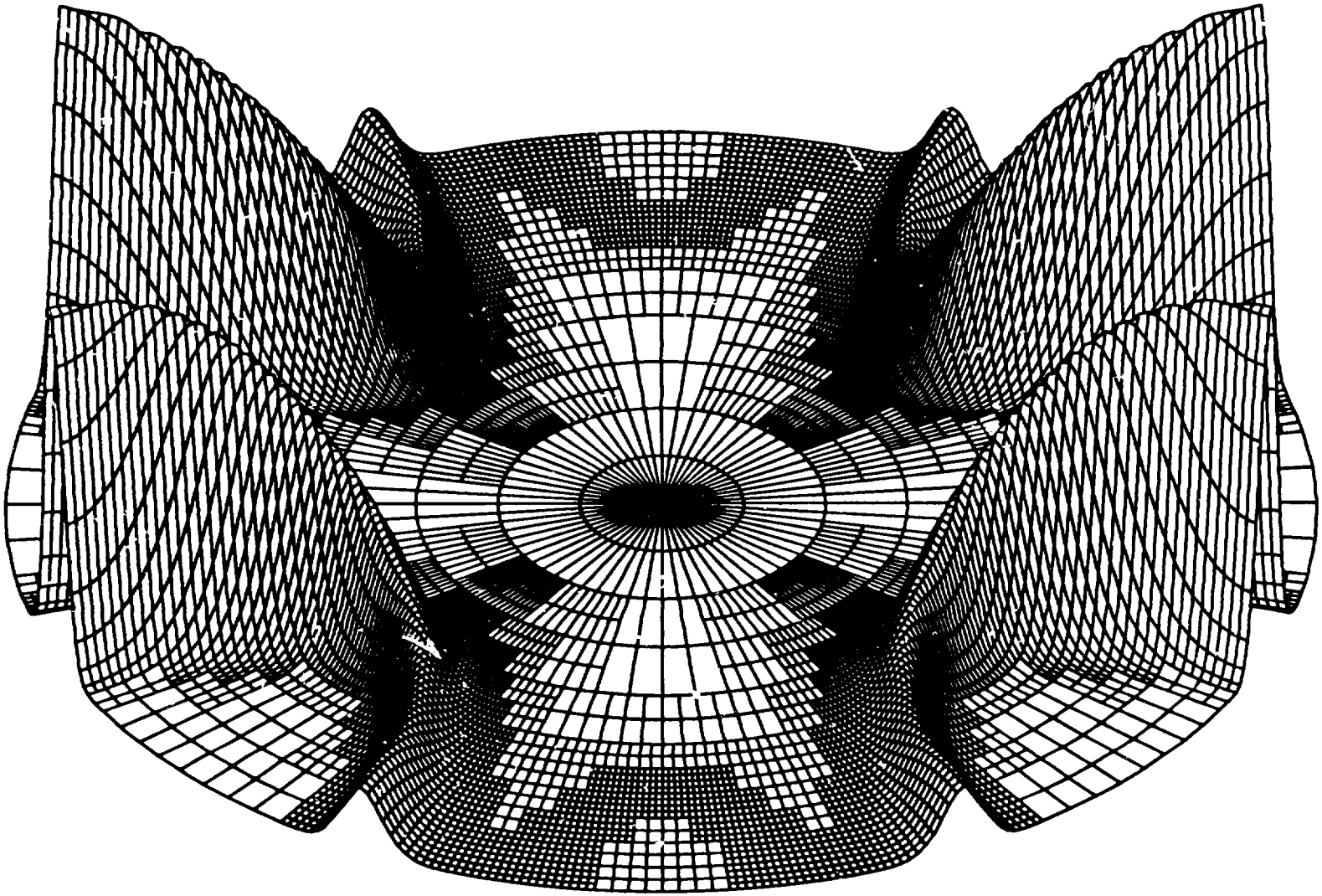

3.5 .

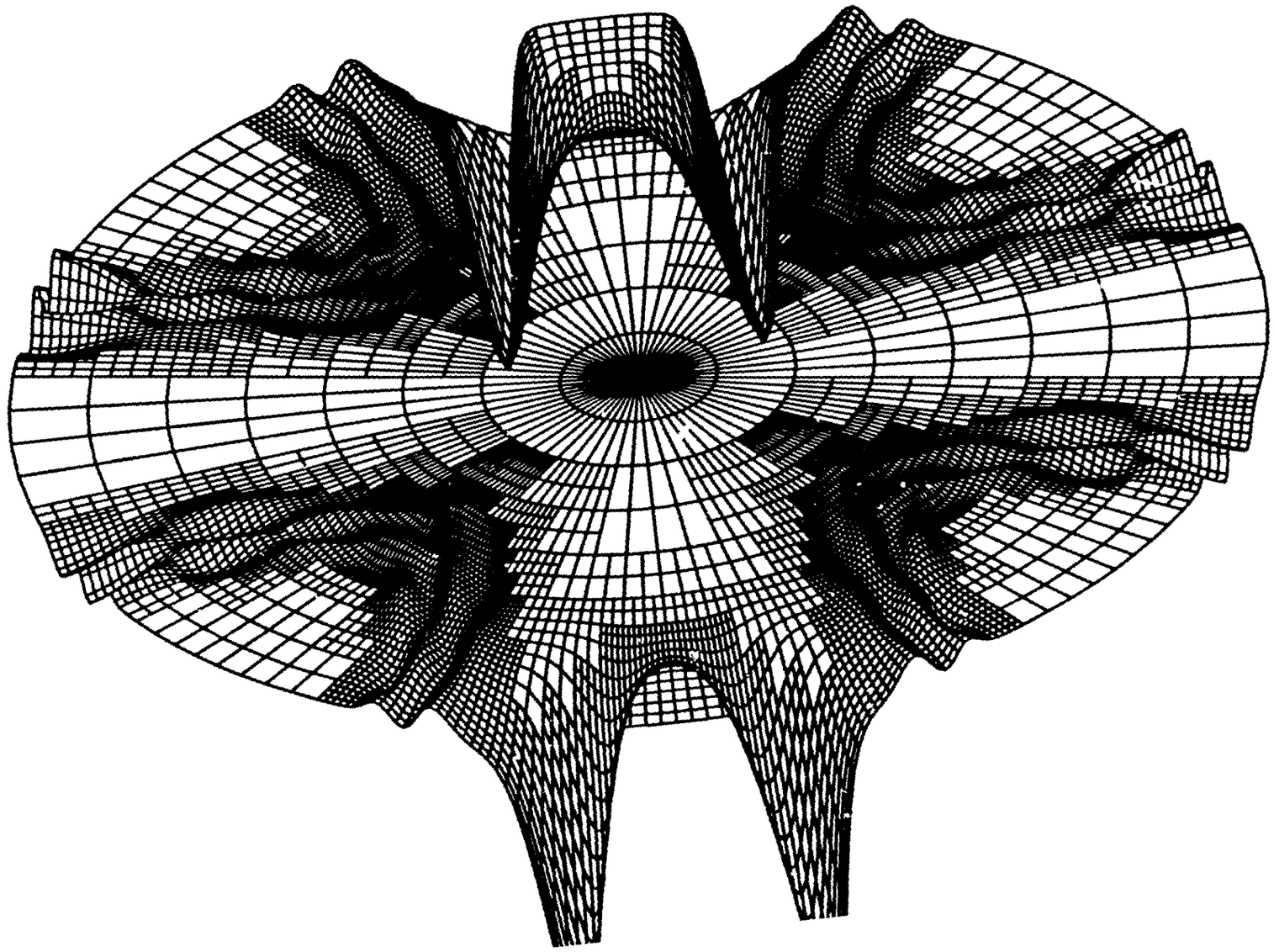

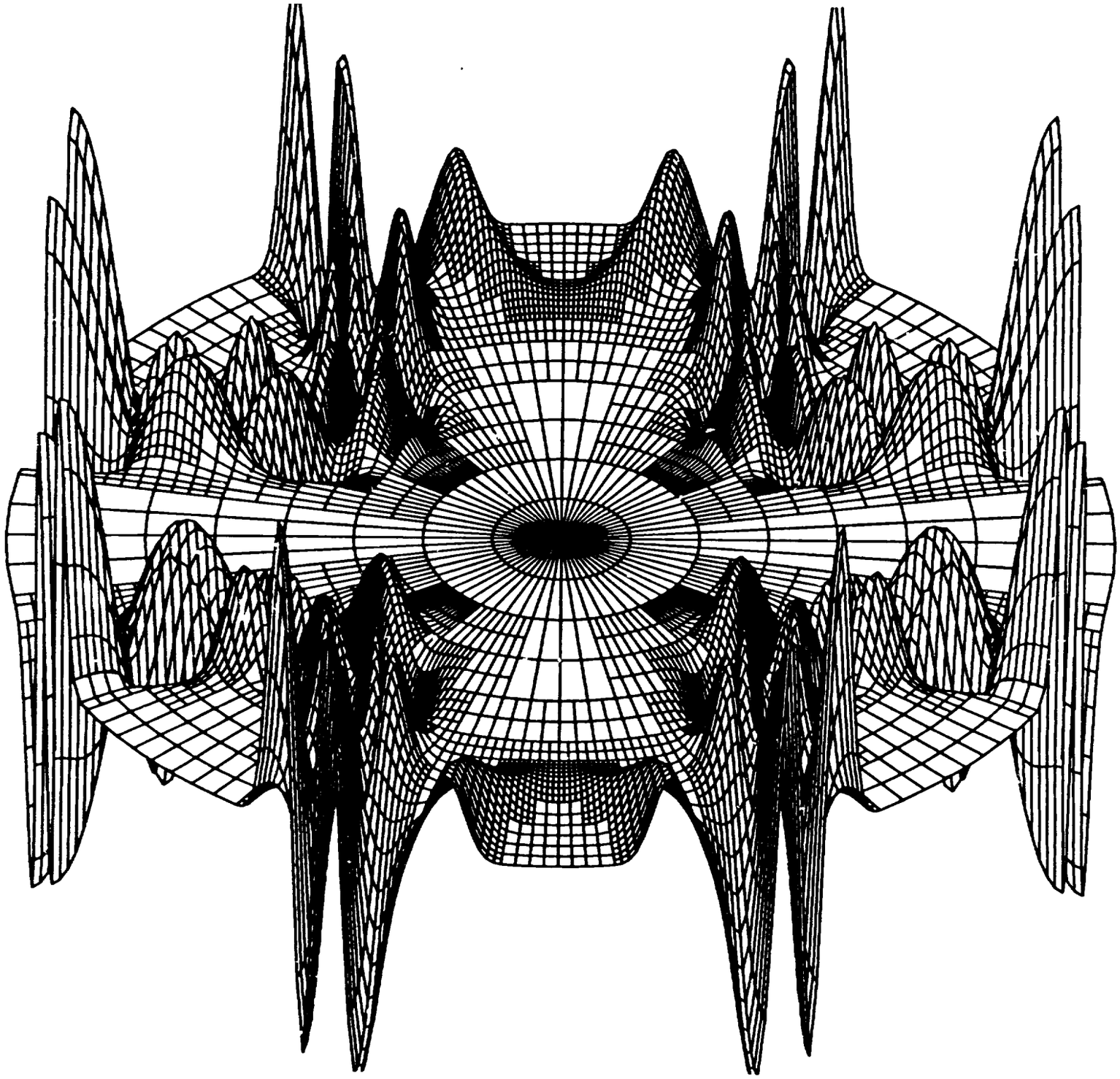

d + μ

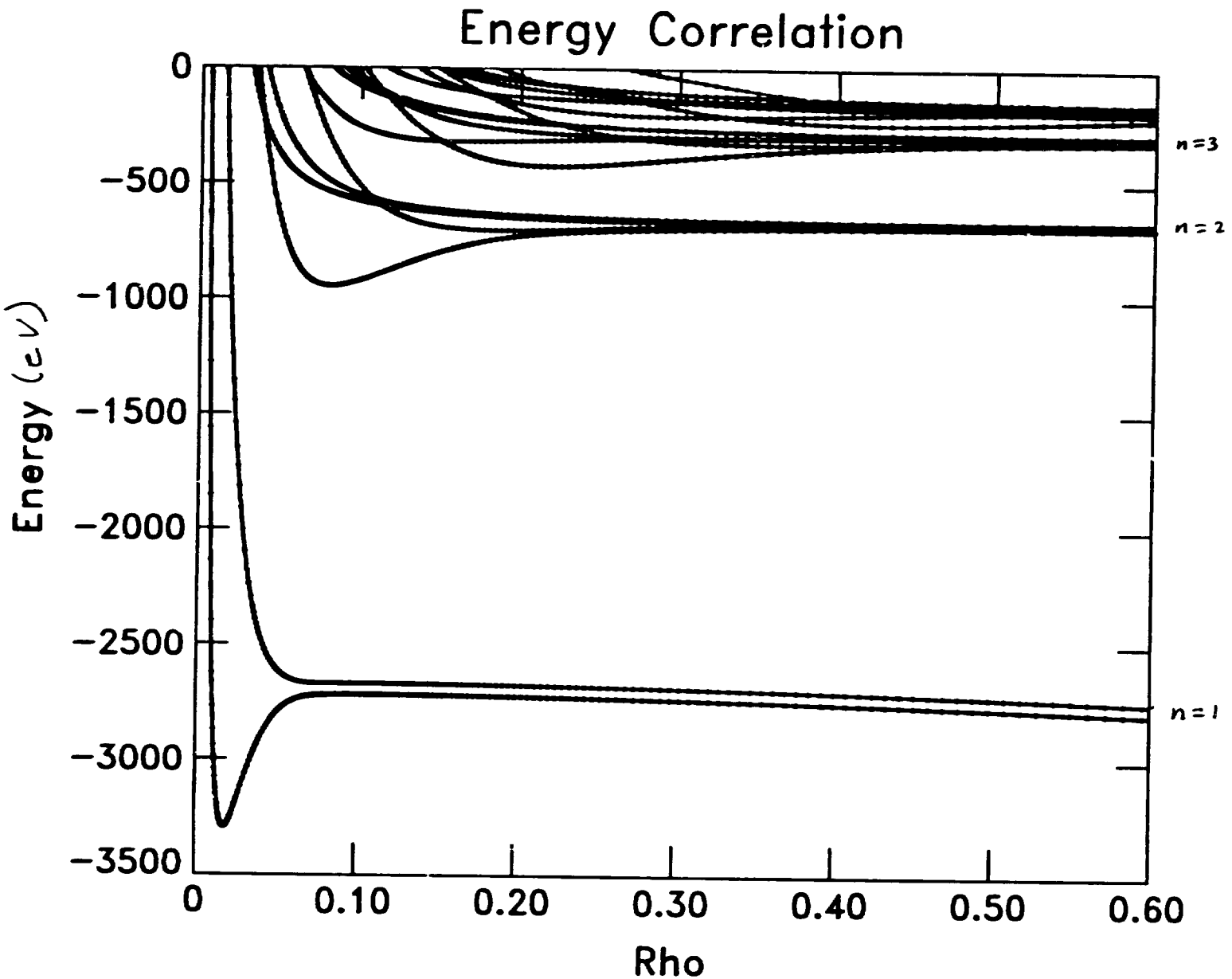
Energy Correlation
0
-500
-1000
-1500
-2000
-2500
-3000
-3500
Energy (eV)
n=3
n=2
n=1
0
0.10
0.20
0.30
0.40
0.50
0.60
Rho

Fig. 4

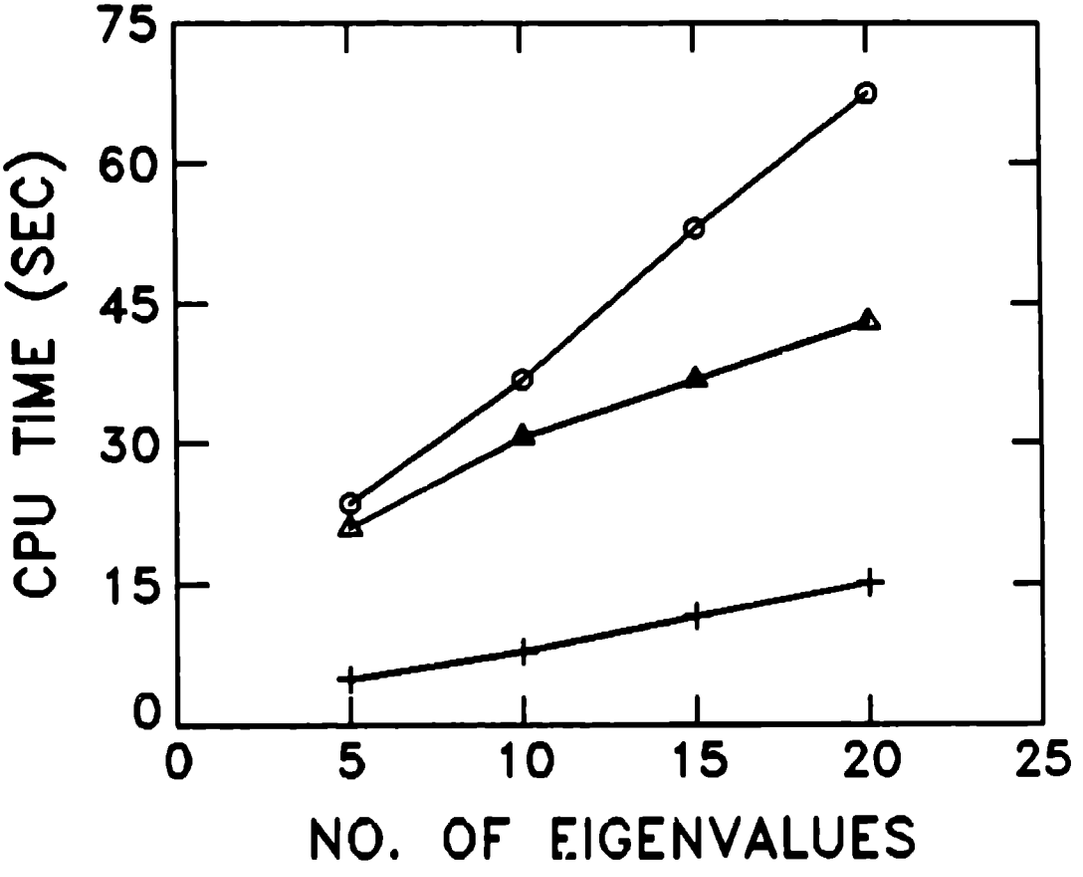

Fig. 6
5

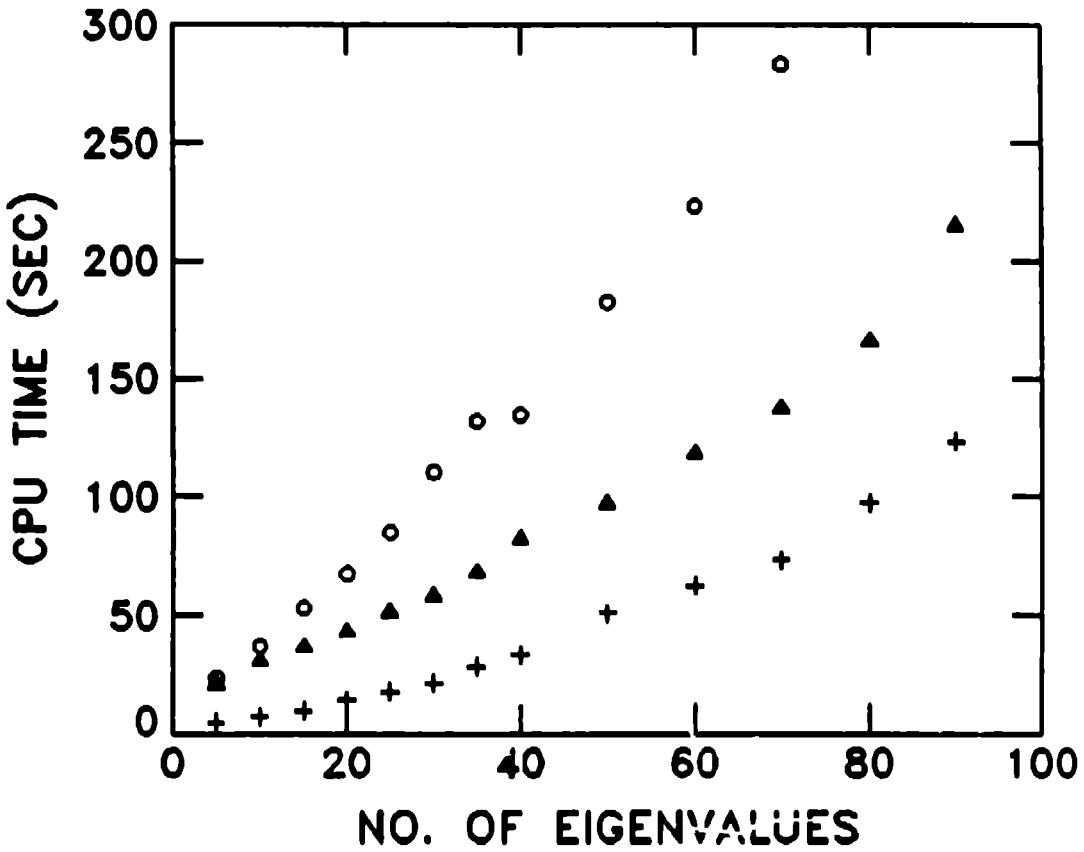
CPU TIME (SEC)
300
250
200
150
100
50
0
0
20
40
60
80
100
NO. OF EIGENVALUES

6a

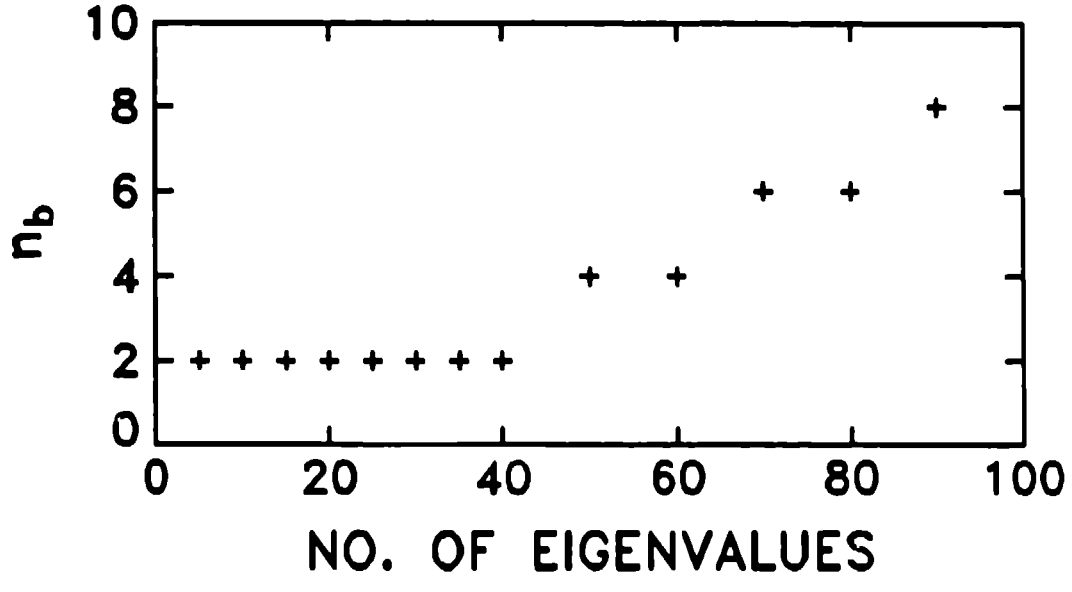
10
8
6
4
2
0
n_b
0
20
40
60
80
100
NO. OF EIGENVALUES